Chapter 16
Magnetism in Nanostructured Spinel Ferrites with Recent Advances in Processing, Characterization, and Applications

Elangbam Chitra Devi and Shougaijam Dorendrajit Singh

1 Introduction

Spinel ferrites have received appreciable attention as an important magnetic material. They have been extensively explored for different applications in different domains of basic and applied sciences because of their certain desirable properties such as magnetic properties, electrical properties, optical properties, thermal and chemical stability. Their potential applications are also expanding to new areas like biomedical applications [1, 2], wastewater treatment [3], sensor technology [4], etc. with the progress in nanoscience and nanotechnology. Based on the Scopus database, research works on spinel ferrites were found to be reported since 1956 along with an exponential increase in the last 20 years which can be seen from Fig. 1.

Also according to the Scopus database, research works on spinel ferrites are found to be investigated in different subject areas which can be seen from Fig. 2. A major contribution comes from Material Sciences followed by Physics and Astronomy, Engineering, Chemistry, Chemical Engineering and a minor contribution from other fields. Although they possess certain desirable properties, most of their applications are found to have relied on their magnetic properties. Their properties are usually tuned by using different strategies such as composition variation, processing conditions, controlling morphologies, reducing size, adopting different preparation methods. This signifies a need for a clear understanding of factors affecting their properties and hence a precise control of their properties and for subjecting to certain applications. New preparation methods with the advancement of nanotechnologies lead toward the production of spinel ferrites into different morphologies with unique magnetic properties. Spinel ferrites of different morphologies such as nanospheres, microspheres, nanofibres, nanorods, nanowires, nanocomposites, core–shell structures were found to be reported by many researchers. Such a wide variety of spinel ferrites were found to be fabricated by different routes of synthesis methods such as

E. C. Devi (✉) · S. D. Singh
Department of Physics, Manipur University, Canchipur, Imphal, Manipur 795003, India

B. P. Swain (ed.), *Advances in Nanostructured Materials*, Materials Horizons: From Nature to Nanomaterials, https://doi.org/10.1007/978-981-16-8391-6_16

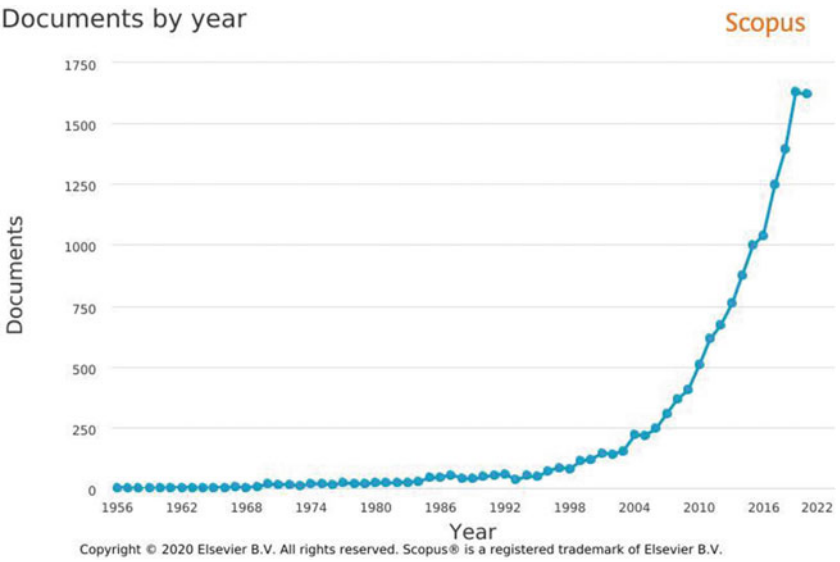

Fig. 1 Publications on spinel ferrites since 1956 based on Scopus database, searched by using keyword "spinel ferrites" on 13th October 2020

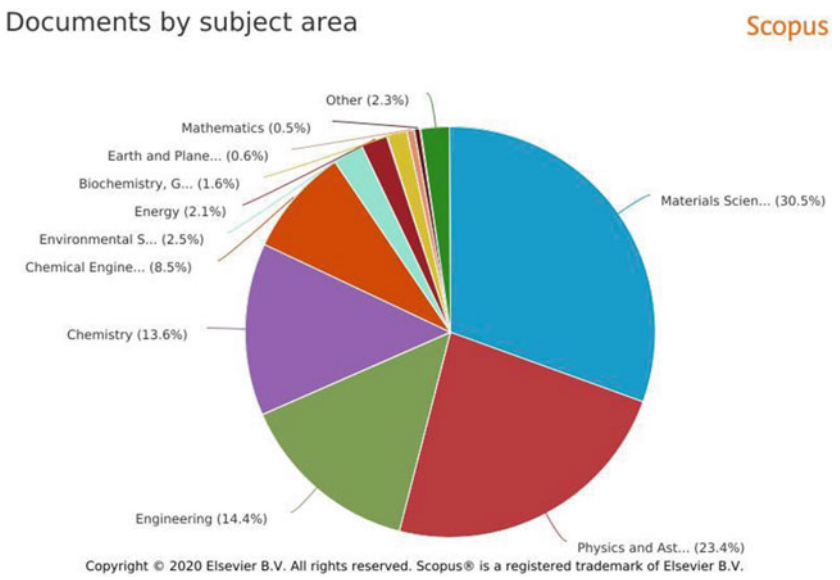

Fig. 2 Percentage of published articles on spinel ferrites contributed from different branches of Science and Engineering based on Scopus database, extracted on 13th October 2020

co-precipitation, hydrothermal, sol–gel, electrospinning, thermal treatment method, etc. Also, emerging research on multifunctional materials consisting of a combination of magnetic spinel ferrites and other material like a luminescent material is found to be reported [5, 6]. The use of microstructural characterization techniques like SEM and TEM effectively provides their morphology which also helps in understanding their associated magnetic properties and hence further tailoring of their properties. This chapter gives a compilation report on research work conducted on nanostructured spinel ferrites, fundamental concepts of their magnetic properties, effects of processing conditions, composition, and morphologies thereby emphasizing their importance and emerging applications.

2 Magnetism in Spinel Ferrites

The unit cell of spinel ferrite (as shown in Fig. 3.) is made up of 8 formula units of AB_2O_4 formed by 32 anions and 24 cations. Nearly cubic close packing of anions offers 64 tetrahedral sites and 32 octahedral sites also called A-sites and B-sites respectively. Only 1/8th of tetrahedral sites and 1/2 of octahedral sites are occupied by cations. The spinel structure is categorized in the space group Fd3m.

The Bravia lattice is a face-centered cubic with a basis formed by two formula units ($2\,AB_2O_4$) [7]. According to the site occupancy of the cations, they are classified as normal, inverse, and mixed spinels. In a normal spinel, divalent ions take A-sites while trivalent ions take B-sites. In the case of inverse spinels, divalent ions take B-sites and trivalent ions are equally distributed between A and B-sites. Spinels having cation distribution between these two extremes are known as mixed spinels.

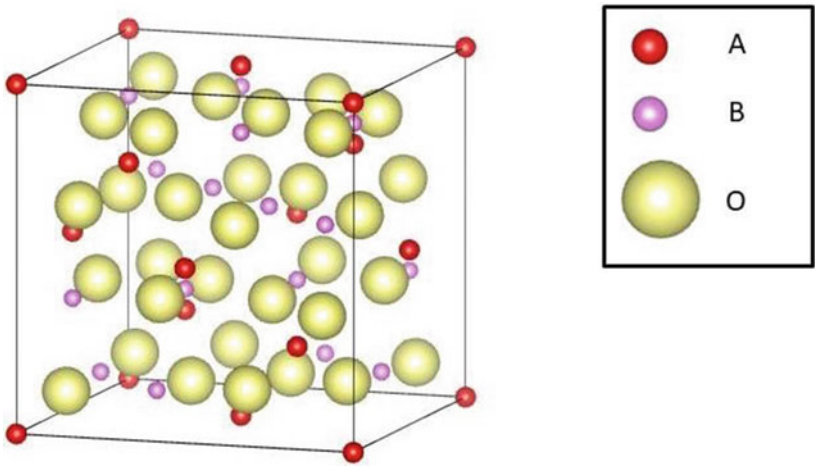

Fig. 3 Spinel structure generated using Vesta

Cation distribution in the spinels is dependent on factors such as temperature, cationic radii, cationic charge, crystal field effects, electrostatic contribution to lattice energy [7]. Cation distribution in spinels is not unique and for any composition of spinel, cation distribution has resulted from an equilibrium of oxygen positional parameter, inversion degree, and lattice constant.

Spinel ferrites have magnetic properties which are found to be greatly dependent on the constituent cations as well as their occupancy in A and B-sites. Using this fact or simply taking into account the magnetic moments associated with the cations and their preference for a specific site, the magnetic properties of spinel ferrites are usually tailored. A variety of spinel ferrites composed of transition metals and rare-earth elements of different compositions are found to be reported, some of which are listed in Table 1. The magnetism in spinel ferrites is found to be originated from the negative interaction or exchange force between the moments of the two cations on different interstitial sites which depends on the distances between the metal–oxygen-metal ions and the angle between them [8]. In general, the interaction is found to be greatest for an angle of 180° and the shortest inter-ionic distance. Three types of interactions are possible namely A-B, B-B, and A-A. Owing to preferable bond angles and lengths in the case of A-B interaction, it is the dominant exchange interaction among the three possible interactions. But, in the case of A-A and B-B interactions, the distances between the oxygen and metal ions are much large and the angle between the metal and oxygen ions are too small. Thus, the magnetic interaction in spinel ferrites, in general, comprises of strong A-B interaction with much weaker B-B interaction and most unfavorable A-A interaction. Neel first explained the ferrimagnetism of ferrites by considering the main negative interaction occurring between A and B-sites and thus developed the theory of ferrimagnetism [8].

3 Materials and Method

Table 1 represents an overview of some of the research works reported in spinel ferrites prepared through different methods and processing conditions giving rise to different sizes and morphologies and their associated magnetic properties. From the table, it can be found that a wide variety of methods are found to be adopted for different types of spinel ferrites ranging from a low-temperature method such as simple co-precipitation methods to conventional methods including high-temperature heat treatments. Desirable magnetic properties are found to be tuned by using a particular synthesis method or processing conditions. Apart from these, composition variation is another factor used for tailoring their properties. Table 1 elucidates that for the varying composition of spinel ferrites and their processing conditions, the important magnetic parameters like saturation magnetization, coercivity, and retentivity values are different. Spinel ferrites of different morphologies ranging from simple spherical nanoparticles to complex structures are found to be reported. Yuan et al. [9] reported studies on $CoFe_2O_4$ microspheres which are composed of assemblies of nanoparticles of $CoFe_2O_4$ of average sizes of 8 nm

Table 1 Spinel ferrites were prepared using different methods under different processing conditions

Composition	Preparation method	Processing condition	Size and Morphology	M_s (emu/g)	H_c (Oe)	References
$Cd_xCo_{1-x}Zr_{0.05}Fe_{1.95}O_4$ x = 0 to 0.30, step size of 0.05	Pechini method	Calcined at 700 °C in air for 1 h	32–40 nm Spherical	57.33–67.89	1120–1500	[25]
$CoLn_{0.12}Fe_{1.88}O_4$ Ln = Ce, Eu, Sm, Dy, Gd, Er	Micelles method	–	~20 nm	65–85	7256–12,112	[26]
$CoFe_2O_4$ encapsulated in mesoporous silica matrices and $CoFe_2O_4$ nanowires	Chemical method	–	2.5–9 nm Encapsulated structures and nanowires	31.9–53.6	–	[27]
$Cd_{0.5-}Ni_xCo_{0.5}Fe_2O_4$	Auto-combustion method	–	7.2–12.9 nm Spherical	33.785–51.311	300–657	[28]
$CoFe_2O_4$ $CoFe_2O_4/SiO_2$	Hydrothermal and sol–gel method	Heated at 1000 °C for 96 h	16 nm and 17 nm Rounded polyhedral morphology	80,2–86.8	–	[29]
$Mn_{0.5}Co_{0,5}Fe_2O_4$	High energy ball milling	100, 200, 300, 400, 500 °C at argon atmosphere	7–11 nm Spherical	29.8–51.0	–	[30]
$CoFe_2O_4$	Solvothermal method		2–15 nm Spherical	256–506	–	[31]
$Co_{1-x}Zn_xFe_2O_4$	Auto-combustion method	Calcined at 800 °C for 3 h Sintered at 1300 °C for 12 h in air	Spherical			[32]

(continued)

Table 1 (continued)

Composition	Preparation method	Processing condition	Size and Morphology	M_s (emu/g)	H_c (Oe)	References
$CoFe_2O_4$	Coprecipitation method	Annealed at 300, 1000, 1300 °C	10 nm Spherical	45–85	1000–5000	[33]
$Co_{0.4+x}Zn_{0.6-x}Fe_2O_4$ and $Co_{0.4+x}Zn_{0.5-x}Li_{0.1}Fe_2O_4$	Sol–gel auto-combustion method	–	13–34 nm Platelets shaped	59.06–148.70 and 56.98–123.32	16–2560 and 114–1476	[34]
$Zn_xCo_{1-x}Fe_2O_4$	Sol–gel method	Annealed at 500 oC and 900 °C for 2 h in air	15–46 nm Spherical	53–116	–	[35]
$Co_{0.5-x}Zn_{0.5}Ni_xFe_2O_4$ x = 0.05 to 0.25, in 0.05 step size	Auto-combustion method	Annealed at 1000 °C for 4 h	34.54- 37.56 nm Spherical	35.3–65.68	–	[36]
$ZnFe_2O_4$	Co-precipitation method	–	5–11 nm Spherical	3–7.3	–	[37]
$ZnFe_2O_4$	Co-precipitation method	–	9.8–13.4 nm	37.6–52.9	–	[38]
$ZnFe_2O_4$ Dispersed in silica aerogel matrix	Chemical method	Heated at 450, 750, 900 °C for 1 h and 750 °C for 6 h	4.2–11.1 nm Dispersed in silica matrix	6.3–9.2	444–786	[39]
$Ni_xMn_{1-x}Fe_2O_4$ x = 0 to 1.0, step size of 0.2	Microwave-assisted combustion method	–	16–19 nm Spherical	35.42–66.93	60.23–111.42	[40]
Fe_3O_4	Colloidal nanocrystal synthesis	–	12 nm Slightly elongated spherical shaped	51	~ 0	[41]

(continued)

Table 1 (continued)

Composition	Preparation method	Processing condition	Size and Morphology	M_s (emu/g)	H_c (Oe)	References
Fe_3O_4	Oxidation reaction method	–	9.6–287 nm Cubic and spherical	54.7–84.7	0–190	[42]
$CaFe_2O_4$	Sol–gel method	–	7.6 nm	27.78–29.92	0–150	[43]
$CaFe_2O_4$	Sol–gel method	Heated at1000 °C for 12 h	6–10 nm	13.2–15.3	–	[44]
$Zn_{1-x}Ni_xFe_2O_4$ x = 0 to 1.0, in 0.2step size	Combustion method	–	30–42 nm	36.77–59.93	24.4–138.7	[45]
$Mn_{0.5}Zn_{0.25}Fe_2O_4$	Co-precipitation method	–	19 nm Spherical	18.4	~ 0	[46]
$Co_{1-x}Zn_xFe_2O_4$	Sol–gel auto-combustion method	–	22.9–34.9 nm Agglomerated, complex grain arrangement	21.8–67.8	175–786	[47]
$Cu_{1-x}Zn_xFe_2O_4$ x = 0 to 0.75, step size of 0.25	Novel nanocasting route	-	6.5–8.3 nm	18–52	40–380	[48]
$NiFe_2O_4$	Microwave-assisted combustion method	Heated for 8 h at 300, 400, 500, 600, 700, 800 °C	3.88–85.16 nm Nearly cubic	1.73–39.39	23–180	[49]
$CuCe_xFe_{2-x}O_4$	Co-precipitation method	Calcined at 600 °C for 6 h, sintered at 950 °C for 6 h	Agglomerated nanoparticles	16.39–37.79	61.26–257.08	[50]

(continued)

Table 1 (continued)

Composition	Preparation method	Processing condition	Size and Morphology	M_s (emu/g)	H_c (Oe)	References
$Cu_xCr_xFe_{2-x}O_4$ x = 0 to 0.5, step size of 0.05	Citrate precursor method Annealed at 600 °C for 2 h	–	23–42 nm Agglomerated nano-structure	17.22–35.32	125–209	[51]
$NiFe_2O_4$	Thermal treatment method	Calcined for 3 h at 623, 673, 723, 823 K	10–51 nm Spherical	0.6–29.05	51–150	[52]
$NiFe_2O_4$	Microwave-assisted combustion method	–	34.7–42 nm Regular and irregular polyhedrons	48.75–60.87	112.62–177.55	[53]
$Zn_xNi_{1-x}Fe_2O_4$	PEG assisted hydrothermal method	–	9.1–27.0 nm Irregular polygonal and regular nanospheres	3.09–80.24	–	[54]
$NiFe_2O_4$	Hydrothermal method	–	51.23 nm Rod-like platelet	16.10		[55]
$Ni_{1-x}Mg_xFe_2O_4$	Co-precipitation method	Annealed at 900 °C	30–40 nm Agglomerated spherical, irregular structured nanoparticles	10.03–28.82	82.85–186.22	[56]
$Zn_{1-x}Mg_xFe_2O_4$ x = 0–1.0, step size of 0.2	Co-precipitation method	Annealed at 900 °C for 5 h in air	21–188 nm Agglomerated nanoparticles	1–34	85–101	[57]

(continued)

Table 1 (continued)

Composition	Preparation method	Processing condition	Size and Morphology	M_s (emu/g)	H_c (Oe)	References
$MgFe_2O_4$	Hydrothermal method	–	8.935 nm Spherical shaped and chain liked clusters	4	–	[58]
$Ni_{0.7-x}Zn_{0.3}M_xFe_2O_4$ $M = Co^{2+}, Mn^{2+}, Cu^{2+}$ $x = 0, 0.1, 0.3, 0.5, 0.7$	Citrate method	–	25.75–54.84 nm Agglomerated nanoparticles with different shapes and sizes	51.3–66.4	76–477	[59]
$CoCr_xFe_{2-x}O_4$ $x = 0–1.0$, step size of 0.25	PVA assisted sol–gel method	Calcined at 350, 500, 700, 1000 °C for 4 h	7–49 nm Cubic like grains	7–78	13–1411	[60]
$Mg_{1-x}Zn_xFe_2O_4$ $x = 0, 0.05, 0.10, 0.15$	Electrospining method	Calcined at 550 °C for 2 h in air	Nanofibers of average diameter 100–350 nm	20.25–29.76	90–96	[61]
$Co_{1-x}Cu_xCe_{0.05}Fe_{1.95}O_4$ $x = 0–1.0$, step size of 0.25	Sol–gel method	Sintered at 700 °C for 5 h	31.25–84.69 nm Nanoparticles with varying shapes	14.13–29.81	240.5–315.89	[62]
$Mg_{0.5}Zn_{0.5-x}Co_xFe_2O_4$ $x = 0$ to 0.500, step size of 0.125	Co-precipitation method	–	36.17–70.13 nm	36.18–59.41	0–883.40	[63]

(continued)

Table 1 (continued)

Composition	Preparation method	Processing condition	Size and Morphology	M_s (emu/g)	H_c (Oe)	References
$NiDy_xFe_{2-x}O_4$	Auto-combustion method	Annealed for 2 at 800 °C h, sintered for 3 h at 1200 °C	39–52 nm Polygonal shaped grains with non-uniform size distribution	43.75–50.07	27.37–58.41	[64]
$NiFe_2O_4$, $Ni_{0.9}Cd_{0.1}Fe_2O_4$, $Ni_{0.9}Sr_{0.1}Fe_2O_4$, $Ni_{0.9}Cd_{0.05}Sr_{0.05}Fe_2O_4$	Auto-combustion method	Calcined at 800 °C for 6 h and sintered at 850 °C for 8 h	26–37 nm	18.34–34.79	183.5–218.59	[65]
$Co_{0.7}Zn_{0.3}Sm_yFe_{2-y}O_4$ x = 0 to 0.04, step size of 0.01	Auto-combustion method	Sintered for 4 h at 450 °C	22–47 nm Closely packed spherical shaped fine grains	7.78–96.83	274–481	[66]
$CuPr_xFe_{2-x}O_4$ x = 0 to 1.0, step size of 0.25	Sol–gel method	Sintered at 750 °C for 6 h	62.31–84.05 nm Agglomerated nanoparticles with irregular shapes	30.37–42.22	295.29–773.82	[67]
$CoY_xFe_{2-x}O_4$ x = 0, 0.1, 0.15, 0.2, 0.3	Auto-ignition method	Sintered at 800 °C for 2 h	37–43 nm Nearly spherical shaped nanoparticles	35.63–72.19	346–684	[68]
$Ni_xCu_{0.1}Zn_{0.9-x}Fe_2O_4$	Co-precipitation method	Heated for 2 h at 800 °C	21.3–23.5 nm Nearly spherical and uniform sized nanoparticles	23.87–38.36	24.09–64.99	[69]

(continued)

Table 1 (continued)

Composition	Preparation method	Processing condition	Size and Morphology	M_s (emu/g)	H_c (Oe)	References
$CoFe_2O_4$	Mechanical milling	Calcined at 1000 °C for 2 h	28–324 nm Agglomerated and irregular shapes	48–78	650–2092	[70]
$CoCe_xDy_xFe_{2-2x}O_4$ x = 0 to 0.05, in 0.01step size	Auto-combustion method	Calcined for 4 h at 400 °C in air	Agglomerated nanoparticles	52–84	245–976	[71]
$CoFe_2O_4$	Reverse co-precipitation method Magnetic field assisted	–	22.44–26.96 nm Agglomerated nanoparticles	54.24–61.22	339.25–385.2	[72]
$Co_xNi_{1-x}Fe_2O_4$ x = 0 to 1.0 in 0.2step size	Sol–gel auto-combustion method	Pre-heated for 1 h at 500 °C and calcined for 2 h at 1200 °C in air	36–58 nm Roughly spherical and beveled edges cubes	50–93	50–650	[73]
$Co_{1-x}Mn_xFe_2O_4$ x = 0, 0.05, 0.10, 0.15, 0.20, 0.25, 0.30	Auto-combustion method	Annealed at 1000 °C for 12 h	22–30 nm	52.55–68.94	604–1592	[74]
$Mn_{1-x}Zn_xFe_2O_4$ x = 0 to 0.5, in 0.1step size	Co-precipitation method	–	10.66–25.96 nm	37.05–58.66	12.59–74.55	[75]
$Mn_{1-x}Ni_xFe_2O_4$ x = 0.1 to 0.5, in 0.1step size	Co-precipitation method	–	21.16–26.38 nm	23.09–60.90	87.616–123.32	[76]

(continued)

Table 1 (continued)

Composition	Preparation method	Processing condition	Size and Morphology	M_s (emu/g)	H_c (Oe)	References
$MnFe_{2-x}La_xO_4$ and $MnFe_{2-x}Gd_xO_4$ x = 0.02 to 0.10, step size of 0.02	Co-precipitation method	–	26.84–32.86 nm ($MnFe_{2-x}La_xO_4$) 26.07–30.88 nm ($MnFe_{2-x}Gd_xO_4$)	50.36–69.1 and 44.10–60.4	107.54–126.69 ($MnFe_{2-x}La_xO_4$) and 100.36–155.08 ($MnFe_{2-x}Gd_xO_4$)	[77]
$NiFe_{2-x}Cr_xO_4$ x = 0 to 1.0, in 0.2 step size	Co-precipitation method	Heated at 837 K for 6 h	20–30 nm	10.18–53.38	16–320	[78]
$Co_{0.7}Zn_{0.3}Tm_xFe_{2-x}O_4$ x = 0 to 0.04, step size of 0.01	Sonochemical method	–	7.37–9.66 nm Agglomerated grains	20.2–28.9	15.5–19.1	[79]

shown in Fig. 4. The microspheres of $CoFe_2O_4$ were prepared using the solvothermal method at different reaction times resulting in the average size distribution of 200 to 330 nm along with transformation from spherical to octahedral shapes. In their studies, 220 nm-sized $CoFe_2O_4$ microspheres composed of 8 nm nanoparticles were found to exhibit superparamagnetism. Li et al. [10] described the preparation of monodispersed $CoFe_2O_4$ nanoparticles using the hydrothermal method (as shown in Fig. 5.). The prepared nanoparticles were nearly spherical shaped with a mean size of 5.5 nm and were found to exhibit superparamagnetism at room temperature. Yang

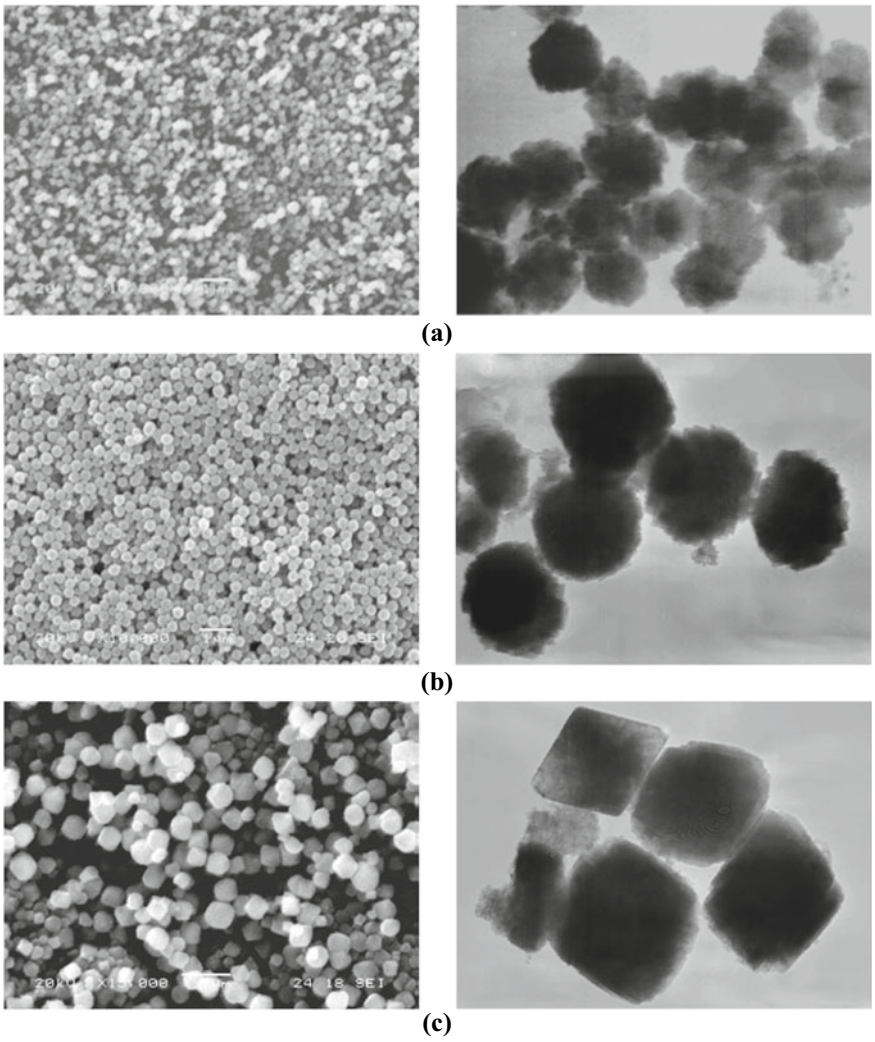

Fig. 4 SEM (left) and TEM (right) images of $CoFe_2O_4$ microspheres prepared using solvothermal method at different reaction time of **a** 12 h, **b** 24 h, **c** 36 h [9]

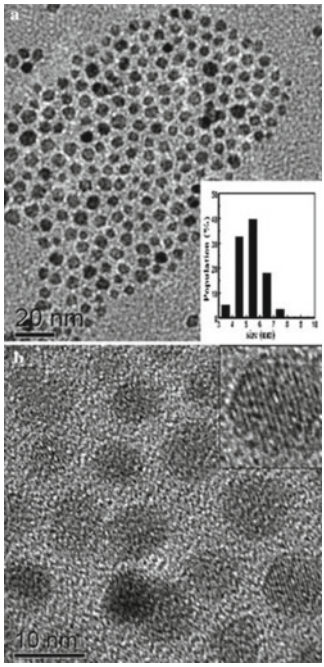

Fig. 5 TEM images of monodispersed $CoFe_2O_4$ nanoparticles prepared using hydrothermal method [10]

et al. [11] fabricated nanorods of Fe_3O_4 which are shown in Fig. 6 and investigated for hyperthermia applications. Gao et al. [12] reported studies on the directional dependency of nanowire arrays of $ZnFe_2O_4$ having about 16 nm diameter ordered in anodic aluminum oxide (AAO) templates that were prepared using the electrodeposition method (shown in Fig. 7). Maensiri et al. [13] reported studies on nanofibres of $MgFe_2O_4$/polyvinyl pyrrolidone (PVP) composites fabricated by the method of electrospinning. Their study shows that the morphology of the nanofibres greatly depends on the calcination temperature. The structural transformation (which is shown in Figs. 8. and 9) from smooth and uniform cross-section nanofibres to a structure of packed crystallites of about 10–20 nm for 700 °C and 25–80 nm for 800 °C calcined samples. Along with the increase in crystallinity, saturation magnetization values

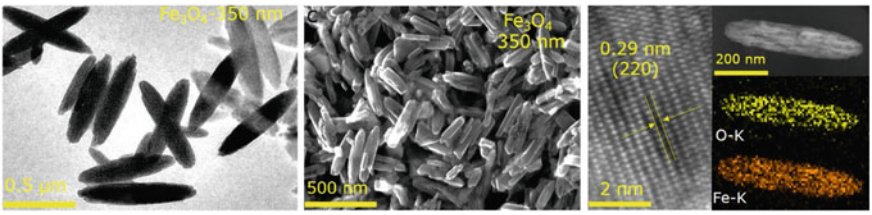

Fig. 6 Images of Fe_3O_4 nanorods prepared using hydrothermal method, TEM (left), SEM (middle), HRTEM (right), adapted from [11]

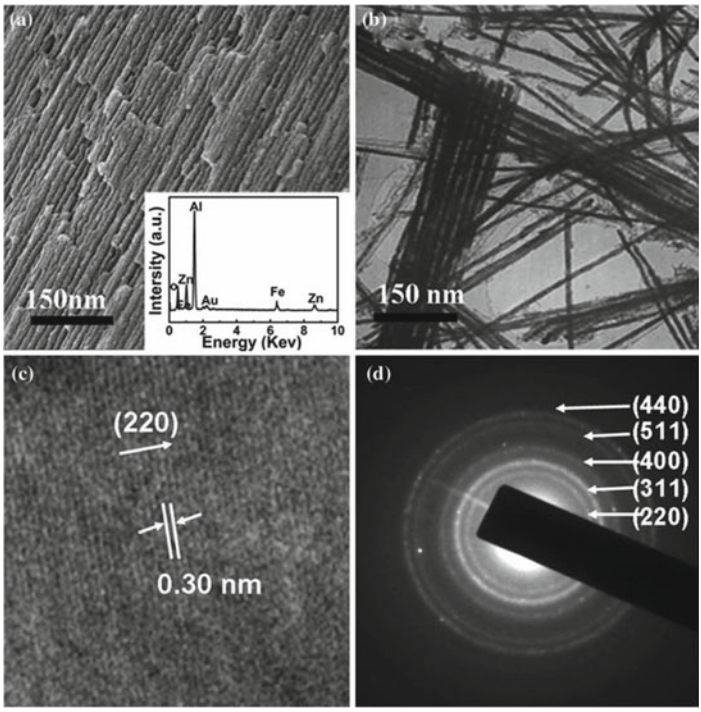

Fig. 7 $ZnFe_2O_4$ nanowires arrays in AAO templates prepared using electrodeposition method **a** SEM, **b** TEM, **c** HRTEM **d** SAED pattern [12]

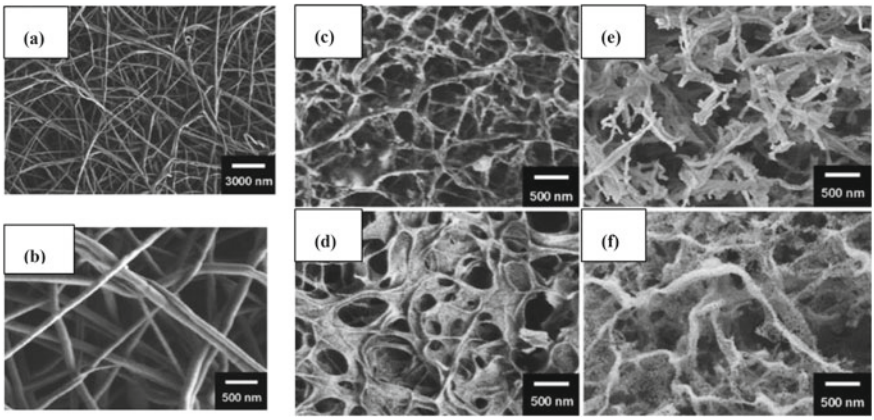

Fig. 8 SEM images of as-spun (**a**), **b** $MgFe_2O_4$/PVP composites and calcined for 2 h in air at **c** 500 °C, **d** 600 °C, **e** 700 °C and **f** 800 °C, adapted from [13]

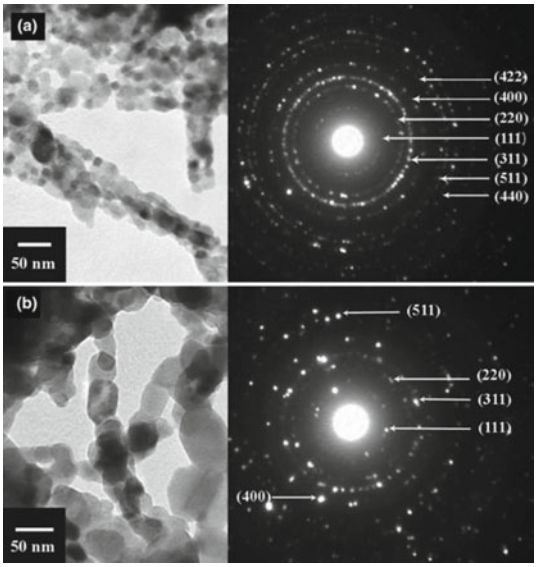

Fig. 9 TEM images and SAED pattern of $MgFe_2O_4$/PVP composites calcined at **a** 700 °C and **b** 800 °C for 2 h in air [13]

were also found to be enhanced with increasing calcination temperature. In addition to these, different structures namely coaxial nanobelts, Janus nanofibres, hollow nanofibers, sandwiched structures, nanorattles, microspheres, core–shell structures formed with other kinds of materials are also found to be reported which are being discussed in Sect. 6.

4 Characterization of Magnetic Properties

4.1 Fundamentals of Magnetization

The fascinating and versatile applications of magnetic materials are based on their magnetization curves or hysteresis loops. Applications of magnetic materials are determined using the knowledge of how they respond to a magnetic field which is represented by their hysteresis loops. It gives information about how magnetic materials take their path when they are subjected to a magnetic field. Magnetic materials are categorized based upon the characteristics of their magnetization curves or hysteresis loops. For instance, a paramagnetic material possesses a weak positive magnetization, showing a linear response when a field is applied. While ferromagnetic and ferrimagnetic types of materials show a non-linear S-shaped magnetization curve with a hysteresis loop. When a magnetic field is applied to ferromagnetic or ferrimagnetic materials, their magnetization increases until it reaches a maximum called saturation magnetization. But when the field is decreased from the saturation region it doesn't return in the same path, rather takes up a new path

retaining some magnetization even after complete removal of the applied field which is termed as retentivity. A field applied in opposite direction can remove the retentivity and is known as coercivity. With the further increase in the applied magnetic field along opposite direction, again saturation will be attained and after increasing the magnetic field along the original direction up to saturation, a complete hysteresis loop is formed. Based upon the coercivity and retentivity, they are categorized as hard and soft magnetic materials. A soft magnetic material refers to those having small values of coercivity and retentivity that are easy to magnetize and demagnetize while hard magnetic materials have the opposite case. Soft magnetic materials are thus found to be used in electromagnets, recording heads, transformer cores, etc. While hard magnetic materials are used in making permanent magnets, memory devices, loudspeakers, etc. [8, 14, 15].

4.2 Theoretical Models

The phenomenon of hysteresis is understood due to the existence of spontaneously magnetized small regions called magnetic domains in ferromagnetic and ferrimagnetic materials [8]. In a demagnetized state, domains are randomly oriented such that the specimen as a whole has zero magnetization but when a magnetic field is applied, they get aligned along the field direction and hence, a net magnetization. The process of magnetization varies in different regions consisting of three main different regions. Starting from the beginning, the 1st region with only reversible magnetization, the 2nd region with an additional non-reversible magnetization, and the 3rd region with reversible magnetization. The magnetization process takes place in two ways, one by magnetic domain wall motion that is the growth of favorably aligned domains at the cost of unfavorably aligned domains and the other by rotation of magnetic domains in the direction of the field applied. At the low field, magnetic domain wall motion dominates while at high field domain rotation dominates and the existence of both in between the two regions. Especially, the high field region of magnetization curves is studied by different forms of the law of approach to saturation. A model represents how basically the magnetization varies with the applied field which is usually expressed proportionally to magnetic field raised with different powers and their combinations [16, 17]. Their dependency and the constant associated with the different field terms give information on their magnetic microstructures, the directional dependency of magnetic properties or magnetic anisotropy, magnetic moments, etc. Increasing research work on tracing the magnetization curves using different models are found to be reported in different types of magnetic materials in different forms, shapes, dimensions for detailed information such as magnetic microstructures, anisotropies, magnetic moments which are intrinsically associated with them [17].

5 Magnetism in Spinel Ferrite Nanoparticles and Their Applications

Magnetic materials had become an indispensable one that covers a wide spectrum of applications like electronic devices, industrial applications, power supply, and storage devices, etc. [14, 15]. In addition, the emergence of nanoscience and nanotechnologies opens up entirely new scientific opportunities. Owing to its interdisciplinary nature, many applications are being extended to different areas like remedies to environmental problems and biomedical applications. It is found that magnetization curves or loops are also dependent on the size of the materials resulting in variation in the models in comparison with their bulk forms. It has been found that in the nano regime, the magnetic materials possess the characteristics of single domain nature which results in the phenomena of superparamagnetism and such materials are termed as superparamagnetic materials [8, 18]. Their behavior is similar to the paramagnetic material that is ideally no retentivity and no coercivity but possesses a much higher magnetization. These are reflected in their magnetization curves and detailed information on their magnetic microstructures can be traced by using suitable models like the Langevin function [19]. Their interesting and spectacular properties lead to new applications such as hyperthermia for cancer treatment, targeted drug delivery, biosensing, enhanced magnetic resonance imaging, etc. thereby widening up the applications of the magnetic materials. For instance, Yang et al. [11] demonstrated the applicability of Fe_3O_4 nanorods for use as magnetic hyperthermia agents. Nanorods of Fe_3O_4 were prepared by hydrothermal method using graphene oxide for avoiding aggregation at different reaction times and post-annealing. Spinel ferrites are also becoming an important candidate for a solution to environmental pollutions. Adsorption based on magnetic separation is desirable because of its effectiveness, low cost, and simple operation process, and hence nanosized spinel ferrites are becoming suitable candidates for adsorption.

Gao et al. [20] investigated the experiment on hollow α-Fe_2O_3 nanofibers for use as a dye adsorbent. In their studies, hollow α-Fe_2O_3 nanofibers were synthesized using a nanofiber template of polyvinyl alcohol by hydrothermal method with calcination. Their studies reported that the α-Fe_2O_3 nanofibers exhibited efficient adsorption of methyl orange present in water along with good magnetic response performance. Zhao et al. [21] studied the adsorption capability of Gd doped Co-ferrites for Congo- red for varying composition of Gd^{3+}. Due to the great surface-to-volume ratio, nano-sized particles exhibit enhanced photocatalytic activity. Ali and Mostafa [22] investigated the photocatalytic activity of Mn-ferrites, Mn-Zn-ferrites, and Mn-Cd-ferrites in reduction of Cr(VI) to Cr(III). Madhubala et al. [23] studied the photocatalytic degradation of dye like methylene blue using Mn-Ni ferrites of 15–20 nm crystallites. Ahalya et al. [24] reported the applicability of Mn-Co-ferrites as adsorbents of Cr(VI). Their results showed the effective adsorption of the heavy metal using spinel ferrites as well as the possibility of reuse of the adsorbent and the heavy metal. Moreover, by combining their properties with other materials in desirable morphologies, new applications in different areas have been reported which are

being discussed in Sect. 6. Better understanding leads to the development of new tricks in expanding their applications. Thus, it can be said that the scenario for the application of magnetic materials is expanding because of more understanding of their behavior.

6 Hybrid-Structured with Other Materials and Their Applications

Apart from the above-discussed applications, magnetic materials are also becoming an important component in multifunctional materials. As magnetic materials can be simply controlled with a magnetic field applied externally, they are also used as an important component in multifunctional materials, vehicles for drug delivery in specific sites inside the human body, and many others. Bifunctional magnetic and luminescent materials are reported to be investigated in biomedical applications such as transporters for drug delivery, agents for MRI, hyperthermia, etc. using simultaneously the magnetic and the luminescent property as the control and tracking respectively. A core–shell structured material comprising of a magnetic core with a luminescent shell occupies an important place in such a class of hybrid-structured materials. For instance, Sun et al. [80] reported multifunctional properties of CdTe quantum dots linked with silica-coated Fe_3O_4 nanoparticles having superparamagnetic properties and their potential applications as immune-labeling with fluorescent imaging of tumor cells. By integrating the magnetic and fluorescent properties into single nanostructured composites their potential applicability as simultaneous targeted drug delivery and bioimaging were investigated. Their studies found that the prepared nanocomposites can be magnetically guided for the delivery of drugs and at the same time their fluorescent property enabled the optical imaging of the nanocomposites and hence with the feasibility of their optical tracing. Atabaev et al. [81] reported fabrication and characterization of bifunctional composites comprising of magnetic Fe_3O_4 particles coated with luminescent Y_2O_3:Tb^{3+} shell. The average size of about 306 to 330 nm magnetic core covered with a phosphor shell of a thickness of about 25 nm was found to exhibit desirable magnetic and luminescent properties suggesting ease for magnetic targeting and separation as well which may find applications in biomedical and bioanalytical applications. Liu et al. [5] investigated bifunctional properties of core–shell Fe_3O_4-CdSe nanoparticles prepared by a polyol process. Magnetic Fe_3O_4 core of about 10 nm diameter covered with CdSe luminescent shell of about 2 nm thicknesses. Sun et al. [82] reported the fabrication of hybrid materials consisting of Fe_3O_4 nanoparticles encapsulated with SiO_2 and functionalized by YVO_4:Eu^{3+} phosphors. The prepared nanocomposites were found to exhibit good ferrimagnetic behavior with a strong red emission. Shi et al. [6] prepared and investigated bifunctional properties of Fe_3O_4@C/YVO_4:Sm^{3+} microspheres synthesized by hydrothermal combined with the sol–gel method. In their work, the carbon layer was used to protect Fe_3O_4 particles from oxidation and

protect the lanthanide-based luminescent shell from quenching of luminescence due to Fe_3O_4. Strong red–orange emission and good ferrimagnetic behavior were observed in their composites. Zhang et al. [83] conducted the studies on nanorattles composed of SiO_2 coated Fe_3O_4 covered with luminescent shells of α-NaYF/Yb, Er which was fabricated using an ion-exchange route for application in targeted chemotherapy. The mesoporous composites were found to possess both upconversion luminescent and magnetic properties along with a high capacity for loading drugs, low cytotoxicity, and excellent cell imaging properties. Yang et al. [84] also reported similar sandwich structured materials having magnetic, mesoporous and luminescent properties. Microspheres of Fe_3O_4 encapsulated with silica and functionalized through YVO_4:Eu^{3+} phosphor deposition which was prepared using a combination of hydrothermal and sol–gel method with heat treatment. The resulted composites were found to possess ordered hexagonal mesoporous, good luminescent properties and high magnetization values and were proposed for using as potential candidates for drug delivery system.

Also, core–shell structures with Fe_3O_4 as cores and other luminescent shells such as YVO_4:Eu^{3+} [85] and Gd_2O_3:Eu^{3+} composites [86] having good magnetic and luminescent properties are also reported. Apart from the core–shell structures, other forms of composites are also found. For instance, Huarac et al. [87] prepared the composites of magnetic Fe_2O_3 and luminescent ZnS: Mn nanoparticles prepared by the co-precipitation method. Highly crystalline two phases were found to coexist in XRD studies and the clusters of nanoparticles of Fe_3O_4 and ZnS: Mn existed side by side from HRTEM studies. In addition to these, nanofibre composites of different types such as core–shell nanofibers, nanobelts, Janus nanofibres are also reported. For instance, using the electrospinning method, flexible hollow nanofibers of Fe_3O_4/$Eu(BA)_3$ phen/PVP [88] and core–shell nanofibres composites of Fe_3O_4/PVP@$NaYF_4$:Yb^{3+}, Er^{3+}/PVP [89] having bifunctional properties were fabricated. Xue et al. [90] reported the fabrication of coaxial nanobelts with tunable bifunctional properties of magnetic and luminescent properties. The composites were composed of the magnetic core of $CoFe_2O_4$/polymethyl methacrylate (PMMA) and photoluminescent shells of [$Tb(BA)_3$(phen) + $Eu(BA)_3$ (phen)]/PMMA synthesized by the electrospinning method. Zhou et al. [91] investigated bifunctional magnetic and luminescent properties of double-stranded nanofibers called Janus nanofibers fabricated by the electrospinning method. A Janus nanofiber is composed of side-by-side assembled two strands of nanofibers, one possessing magnetic properties and the other one having luminescent properties. It was found that they have superior luminescent and magnetic properties owing to their special nanostructures and tunable colors based on their composition. Their work demonstrated an approach for the preparation of composites of controlled and tunable luminescent properties, expected to find applications in magnetic nano-bio-label and anti-counterfeit materials, etc. Thus, nanocomposites having combined properties such as magnetically responsive and luminescent properties with different morphologies were proposed to find applications in biomedical applications like drug delivery, targeting on specific sites, bio-separation, and diagnostic applications.

7 Conclusion

To conclude, it can be summarized that the ever-increasing research work on spinel ferrites and their applications in different fields can be observed with the exposure of nanoscience. A variety of compositions of spinel ferrites in different morphologies were fabricated and investigated through different experimental approaches of nanotechnology. Spinel ferrites of different types, compositions, and their composites of different morphologies were found to be fabricated by different routes of synthesis such as co-precipitation, auto combustion, sol–gel, thermal decomposition, microemulsion, hydrothermal, solvothermal method, and electrospinning method. In addition to their composition, their properties also depend on a particular method, specific processing conditions, and morphologies. Spinel ferrites of desirable nanostructured morphologies have been able to realize using advanced techniques in fabrication and microscopy at nano levels. These advanced nanostructured materials on the other hand lead toward new emerging applications which extend to many multidisciplinary areas such as dye degradation, adsorption of heavy metals, drug delivery, hyperthermia applications. Nanoscience and nanotechnology also lead toward the development of hybrid-structured materials possessing bifunctional properties. As a magnetic component in bifunctional materials, Fe_3O_4 has been reported to be successfully used by many researchers. So, it is desirable to extend the investigation also to other varieties of spinel ferrites. Moreover, the development of advanced bifunctional materials could lead toward device miniaturization, designing of cost-effective and energy-efficient devices, etc. The combination of magnetic materials with other different properties will open up new exciting applications in addition to the improvement in the existing applications.

Acknowledgements The author Elangbam Chitra Devi expresses her gratitude to the UGC, New Delhi, India for the award of UGC-DSKPDF (F. 4-2/2006(BSR)/PH/18-19/0090).

References

1. Amiri M, Salavati-niasari M, Akbari A (2019) Magnetic nanocarriers: evolution of spinel ferrites for medical applications. Adv Colloid Interface Sci 265:29–44
2. Kefeni KK, Msagati TAM, Ti T, Mamba BB (2020) Spinel ferrite nanoparticles and nanocomposites for biomedical applications and their toxicity. Mater Sci Eng C 107:110314
3. Reddy DHK, Yun YS (2016) Spinel ferrite magnetic adsorbents: alternative future materials for water purification. Coord Chem Rev 315:90–111
4. Wu K, Li J, Zhang C (2019) Zinc ferrite based gas sensors: a review. Ceram Int 45: 11143–11157
5. Liu H, Wu J, Min JH, Lee JH, Kim YK (2019) Synthesis and characterization of magnetic-luminescent Fe3O4–CdSe core-shell nanocrystals. Electron Mater Lett 15:102–110
6. Shi J, Tong L, Ren X, Li Q, Ding H, Yang H (2013) Bifunctional Fe3O4@C/YVO4:Sm3+ composites with the core-shell structure. Mater Chem Phys 139:73–78
7. Sickafus KE, Wills JM, Grimes NW (1999) Structure of spinel. J Am Ceram Soc 82:3279–3292
8. Cullity BD, Graham CD (2011) Introduction to magnetic materials. Wiley, Hoboken, New Jersey
9. Yuan HL, Wang YQ, Zhou SM, Liu LS, Chen XL, Lou SY, Yuan RJ, Hao YM, Li N (2010) Low-Temperature preparation of superparamagnetic CoFe 2O 4 microspheres with high saturation magnetization. Nanoscale Res Lett 5:1817–1821
10. Li XH, Xu CL, Han XH, Qiao L, Wang T, Li FS (2010) Synthesis and magnetic properties of nearly monodisperse CoFe2O4 nanoparticles through a simple hydrothermal condition. Nanoscale Res Lett 5:1039–1044
11. Yang Y, Huang M, Qian J, Gao D, Liang X (2020) Tunable Fe3O4 nanorods for enhanced magnetic hyperthermia performance. Sci Rep 10:1–7
12. Gao D, Shi Z, Xu Y, Zhang J, Yang G, Zhang J, Wang X, Xue D (2010) Synthesis, magnetic anisotropy and optical properties of preferred oriented zinc ferrite nanowire arrays. Nanoscale Res Lett 5:1289–1294
13. Maensiri S, Sangmanee M, Wiengmoon A (2009) Magnesium ferrite (MgFe2O4) nanostructures fabricated by electrospinning. Nanoscale Res Lett 4:221–228
14. Goldman A (2006) Modern ferrite technology. Springer, USA
15. Chikazumi S (1997) Physics of ferromagnetism. Oxford University Press, New York
16. Devi EC, Soibam I (2019) Law of approach to saturation in Mn–Zn ferrite nanoparticles. J Supercond Nov Magn 32:1293–1298
17. Devi EC, Singh SD (2021) Tracing the magnetization curves: a review on their importance strategy, and outcomes. J Supercond Novel Magn 34:15–25
18. Bedanta S, Kleemann W (2009) Supermagnetism. J Phys D Appl Phys 42:013001
19. Devi EC, Singh SD (2021) Manifestation of magnetic characteristics of zinc ferrite nanoparticles using the Langevin function. J Supercond Nov Magn 34:617–622
20. Gao Q, Luo J, Wang X, Gao C, Ge M (2015) Novel hollow α-Fe2O3 nanofibers via electrospinning for dye adsorption. Nanoscale Res Lett 10:1–8
21. Zhao X, Wang W, Zhang Y, Wu S, Li F, Liu JP (2014) Synthesis and characterization of gadolinium doped cobalt ferrite nanoparticles with enhanced adsorption capability for Congo Red. Chem Eng J 250:164–174
22. Othman AI, Mostafa AG (2015) Photocatalytic reduction of chromate oxyanions on MMnFe2O4 (M=Zn, Cd) nanoparticles. Mater Sci Semicond Process 33:189–198
23. Madhubala G, Manikandan A, Arul AS, Ramar P (2016) Photocatalytic degradation of methylene blue dye and magneto-optical studies of magnetically recyclable spinel NixMn1-xFe2O4 (x = 0.0–1.0) nanoparticles. J Mol Struct 1113: 79–87
24. Ahalya K, Suriyanarayanan N, Ranjithkumar V (2014) Effect of cobalt substitution on structural and magnetic properties and chromium adsorption of manganese ferrite nanoparticles. J Magn Magn Mater 372:208–213
25. Motavallian P, Abasht B, Mirzaee O, Abdollah-Pour H (2019) Correlation between structural and magnetic properties of substituted (Cd, Zr) cobalt ferrite nanoparticles. Chin J Phys 57:6–13

26. Kahn ML, Zhang ZJ (2001) Synthesis and magnetic properties of CoFe2O4 spinel ferrite nanoparticles doped with lanthanide ions. Appl Phys Lett 78:3651–3653
27. Virumbrales M, Blanco-Gutiérrez V, Delgado-Cabello A, Sáez-Puche R, Torralvo MJ (2018) Superparamagnetism in CoFe2O4 nanoparticles: an example of a collective magnetic behavior dependent on the medium. J Alloys Compd 767:559–566
28. Coutinho DM, Verenkar VMS (2019) Spin canting and surface spin disorder in Ni substituted Co-Cd ferrite nanoparticles synthesized by fuel deficient combustion method. J Alloys Compd 782:392–403
29. Blanco-Gutiérrez V, Climent-Pascual E, Sáez-Puche R, Torralvo-Fernández MJ (2016) Temperature dependence of superparamagnetism in CoFe2O4 nanoparticles and CoFe2O4/SiO2 nanocomposites. Phys Chem Chem Phys 18:9186–9193
30. Moyo HMIAT (2013) The influence of annealing temperature on the magnetic properties of Mn 0.5 Co 0.5 Fe2O4 Nanoferrites synthesized via mechanical milling method. J Supercond Novel Magn 26:1361–1367
31. Vázquez-Vázquez C, López-Quintela MA, Buján-Núñez MC, Rivas J (2011) Finite size and surface effects on the magnetic properties of cobalt ferrite nanoparticles. J Nanoparticle Res 13:1663–1676
32. Nlebedim IC, Vinitha M, Praveen PJ, Das D, Jiles DC (2013) Temperature dependence of the structural, magnetic, and magnetostrictive properties of zinc-substituted cobalt ferrite. J Appl Phys 113:193904
33. Liu BH, Ding J (2006) Strain-induced high coercivity in CoFe2 O4 powders. Appl Phys Lett 88:042506
34. Lal G, Punia K, Dolia SN, Alvi PA, Choudhary BL, Kumar S (2020) Structural, cation distribution, optical and magnetic properties of quaternary Co0.4+xZn0.6-xFe2O4 (x = 0.0, 0.1 and 0.2) and Li doped quinary Co0.4+xZn0.5-xLi0.1Fe2O4 (x = 0.0, 0.05 and 0.1) nanoferrites. J Alloys Compd 828:154388
35. Chithra M, Anumol CN, Sahu B, Sahoo SC (2017) Structural and magnetic properties of ZnXCo1−XFe2O4 nanoparticles: nonsaturation of magnetization. J Magn Magn Mater 424:174–184
36. Prasad BBVSV, Ramesh KV, Srinivas A (2018) Structural and soft magnetic properties of nickel-substituted Co-Zn nanoferrites. J Supercond Nov Magn 31:3223–3237
37. Mendonça EC, Jesus CBR, Folly WSD, Meneses CT, Duque JGS (2013) Size effects on the magnetic properties of ZnFe2O4 nanoparticles. J Supercond Nov Magn 26:2329–2331
38. Choi EJ, Ahn Y, Hahn EJ (2008) Size dependence of the magnetic properties in superparamagnetic zinc-ferrite nanoparticles. J Korean Phys Soc 53:2090–2094
39. Thomas JJ, Shinde AB, Krishna PSR, Kalarikkal N (2013) Temperature-dependent neutron diffraction and Mössbauer studies in zinc ferrite nanoparticles. Mater Res Bull 48:1506–1511
40. Madhubala G, Manikandan A, Arul Antony S, Ramar P (2016) Photocatalytic degradation of methylene blue dye and magneto-optical studies of magnetically recyclable spinel NixMn1-xFe2O4(x = 0.0–1.0) nanoparticles. J Mol Struct 1113:79–87
41. Manohar A, Krishnamoorthi C (2017) Low Curie-transition temperature and superparamagnetic nature of Fe3O4 nanoparticles prepared by colloidal nanocrystal synthesis. Mater Chem Phys 192:235–243
42. Li Q, Kartikowati CW, Horie S, Ogi T, Iwaki T, Okuyama K (2017) Correlation between particle size/domain structure and magnetic properties of highly crystalline Fe3O4 nanoparticles. Sci Rep 7:9894
43. Lal G, Punia K, Dolia SN, Alvi PA, Dalela S, Kumar S (2019) Rietveld refinement, Raman, optical, dielectric, Mössbauer and magnetic characterization of superparamagnetic fcc-CaFe2O4 nanoparticles. Ceram Int 45:5837–5847
44. Samariya A, Dolia SN, Prasad AS, Sharma PK, Pareek SP, Dhawan MS, Kumar S (2013) Size dependent structural and magnetic behaviour of CaFe2O 4. Curr Appl Phys 13:830–835
45. El-fadl AA, Hassan AM, Mahmoud MH, Tatarchuk T, Yaremiy IP, Gismelssed AM, Ahmed MA (2019) Nanoparticles synthesized by microwave combustion method. J Magn Magn Mater 471:192–199

46. Debnath S, Deb K, Saha B, Das R (2019) X-ray diffraction analysis for the determination of elastic properties of zinc-doped manganese spinel ferrite nanocrystals (Mn0.75Zn0.25Fe2O4), along with the determination of ionic radii, bond lengths, and hopping lengths. J Phys Chem Solids 134:105–114
47. Barrera G, Coisson M, Celegato F, Raghuvanshi S, Mazaleyrat F, Kane SN, Tiberto P (2018) Cation distribution effect on static and dynamic magnetic properties of Co1-xZnxFe2O4 ferrite powders. J Magn Magn Mater 456:372–380
48. Najmoddin N, Beitollahi A, Kavas H, Majid MS, Rezaie H, Åkerman J, Toprak MS (2014) XRD cation distribution and magnetic properties of mesoporous Zn-substituted CuFe2O4. Ceram Int 40:3619–3625
49. Karcıoğlu KZ, Boncukcuoğlu R, Karakaş IH, Ertuğrul M (2015) The effects of heat treatment on the synthesis of nickel ferrite (NiFe2O4) nanoparticles using the microwave assisted combustion method. J Magn Magn Mater 374:298–306
50. Roman T, Pui A, Lukacs AV, Cimpoesu N, Lupescu S, Iulian A, Kordatos K, Ntziouni A, Postolache P, Zaharia M, Stanciu S, Mito L (2019) Structural changes of cerium doped copper ferrites during sintering process and magneto-electrical properties assessment. Ceram Int 45:17243–17251
51. Heiba ZK, Maher A, Bakr M (2017) Structural analysis and magnetic properties of biphasic chromium-substituted copper ferrites. J Mol Struct 1147:668–675
52. Goodarz M, Saion EB, Abbastabar H, Hashim M, Halim A (2011) Simple preparation and characterization of nickel ferrite nanocrystals by a thermal treatment method. Powder Technol 212:80–88
53. Kooti M, Sedeh AN (2013) Synthesis and characterization of NiFe2O4 magnetic nanoparticles by combustion method. J Mater Sci Technol 29:34–38
54. Kavas H, Baykal A, Toprak MS, Köseoğlu Y, Sertkol M, Aktaş B (2009) Cation distribution and magnetic properties of Zn doped NiFe2O4 nanoparticles synthesized by PEG-assisted hydrothermal route. J Alloys Compd 479:49–55
55. Amiri M, Pardakhti A, Ahmadi-zeidabadi M, Akbari A (2018) Colloids and surfaces B: biointerfaces magnetic nickel ferrite nanoparticles: green synthesis by Urtica and therapeutic effect of frequency magnetic field on creating cytotoxic response in neural cell lines. Colloids Surf B Biointerfaces 172:244–253
56. Moradmard H, Shayesteh SF, Tohidi P, Abbas Z, Khaleghi M (2015) Structural, magnetic and dielectric properties of magnesium doped nickel ferrite nanoparticles. J Alloys Compd 650:116–122
57. Nadeem K, Rahman S, Mumtaz M (2015) Effect of annealing on properties of Mg doped Zn-ferrite nanoparticles. Prog Nat Sci Mater Int 25:111–116
58. Meidanchi A, Motamed A (2020) Preparation, characterization and in vitro evaluation of magnesium ferrite superparamagnetic nanoparticles as a novel radiosensitizer of breast cancer cells. Ceram Int 46:17577–17583
59. Abu-Elsaad NI, Nawara AS, Mazen SA (2020) Synthesis, structural characterization, and magnetic properties of Ni–Zn nanoferrites substituted with different metal ions (Mn2+, Co2+, and Cu2+). J Phys Chem Solids 146:109620
60. Nikmanesh H, Eshraghi M, Karimi S (2019) Cation distribution, magnetic and structural properties of CoCrxFe2-xO4: effect of calcination temperature and chromium substitution. J Magn Magn Mater 471:294–303
61. Ghazi N, Mahmoudi CH, Ghodsi FE (2018) Rietveld refinement, morphology analysis, optical and magnetic properties of magnesium-zinc ferrite nanofibers. J Magn Magn Mater 468:132–140
62. Akhtar MN, Khan AA, Akhtar MN, Ahmad M, Khan MA (2019) Structural rietveld refinement, morphological and magnetic features of Cu doped Co–]Ce nanocrystalline ferrites for high frequency applications. Phys B Condens Matter 561:121–131
63. Sharma R, Thakur P, Kumar M, Thakur N, Negi NS, Sharma P, Sharma V (2016) Improvement in magnetic behaviour of cobalt doped magnesium zinc nano-ferrites via co-precipitation route. J Alloys Compd 684:569–581

64. Chauhan L, Singh N, Dhar A, Kumar H, Kumar S, Sreenivas K (2017) Structural and electrical properties of Dy3+ substituted NiFe2O4 ceramics prepared from powders derived by combustion method. Ceram Int 53:8378–8390
65. Tiwari R, De M, Tewari HS, Ghoshal SK (2020) Structural and magnetic properties of tailored NiFe2O4 nanostructures synthesized using auto-combustion method. Results Phys 16:102916
66. Mugutkar AB, Gore SK, Tumberphale UB, Jadhav VV, Mane RS, Patange SM, Shirsath SE, Jadhav SS (2020) Role of composition and grain size in controlling the structure sensitive magnetic properties of Sm3+ substituted nanocrystalline Co-Zn ferrites. J Rare Earths 38:1069–1075
67. Akhtar MN, Babar M, Qamar S, Rehman Z, Khan MA (2019) Structural Rietveld refinement and magnetic features of prosademium (Pr) doped Cu nanocrystalline spinel ferrites. Ceram Int 45:10187–10195
68. Chakrabarty S, Dutta A, Pal M (2018) Effect of yttrium doping on structure, magnetic and electrical properties of nanocrystalline cobalt ferrite. J Magn Magn Mater 461:69–75
69. Ramakrishna KS, Srinivas C, Meena SS, Tirupanyam BV, Bhatt P, Yusuf SM, Prajapat CL, Potukuchi DM, Sastry DL (2017) Investigation of cation distribution and magnetocrystalline anisotropy of NixCu0.1Zn0.9−xFe2O4 nanoferrites: role of constant mole percent of Cu2+ dopant in place of Zn2+. Ceram Int 43:7984–7991
70. Mahdikhah V, Ataie A, Babaei A, Sheibani S, Yang CWO, Abkenar SK (2019) Control of structural and magnetic characteristics of cobalt ferrite by post-calcination mechanical milling. J Phys Chem Solids 134:286–294
71. Hashim M, Raghasudha M, Meena SS, Shah J, Shirsath SE, Kumar S, Ravinder D, Bhatt P, Alimuddin KR, Kotnala RK (2018) Influence of rare earth ion doping (Ce and Dy) on electrical and magnetic properties of cobalt ferrites. J Magn Magn Mater 449:319–327
72. Samadi MS, Shokrollahi H, Zamanian A (2018) The magnetic-field-assisted synthesis of the Co-ferrite nanoparticles via reverse co-precipitation and their magnetic and structural properties. Mater Chem Phys 215:355–359
73. Torkian S, Ghasemi A, Shoja RR (2017) Cation distribution and magnetic analysis of wideband microwave absorptive CoxNi1−xFe2O4 ferrites. Ceram Int 43:6987–6995
74. Yadav SP, Shinde SS, Bhatt P, Meena SS, Rajpure KY (2015) Distribution of cations in Co1-xMnxFe2O4 using XRD, magnetization and Mössbauer spectroscopy. J Alloys Compd 646:550–556
75. Devi EC, Soibam I (2017) Effect of Zn doping on the structural, electrical and magnetic properties of MnFe2O4 nanoparticles. Indian J Phys 91:861–867
76. Devi EC, Soibam I (2019) Magnetic properties and law of approach to saturation in Mn-Ni mixed nanoferrites. J Alloys Compd 772:920–924
77. Devi EC, Soibam I (2019) Tuning the magnetic properties of a ferrimagnet. J Magn Magn Mater 469:587–592
78. Patange SM, Shirsath SE, Jadhav SS, Jadhav KM (2012) Cation distribution study of nanocrystalline NiFe 2-xCrxO4 ferrite by XRD, magnetization and Mössbauer spectroscopy. Phys Status Solidi Appl Mater Sci 209:347–352
79. Almessiere MA, Slimani Y, Kurtan U, Guner S, Sertkol M, Shirsath SE, Akhtar S, Baykal A, Ercan I (2019) Structural, magnetic, optical properties and cation distribution of nanosized Co0.7Zn0.3TmxFe2−xO4 ($0.0 \leq x \leq 0.04$) spinel ferrites synthesized by ultrasonic irradiation. Ultrason Sonochem 58:104638
80. Sun P, Zhang H, Liu C, Fang J, Wang M, Chen J, Zhang J, Mao C, Xu S (2010) Preparation and characterization of Fe3O4/CdTe magnetic/fluorescent nanocomposites and their applications in immuno-labeling and fluorescent imaging of cancer cells. Langmuir 26:1278–1284
81. Atabaev TS, Kim HK, Hwang YH (2013) Fabrication of bifunctional core-shell Fe3O4 particles coated with ultrathin phosphor layer. Nanoscale Res Lett 8:357
82. Sun Z, Liu D, Tong L, Shi J, Yang X, Yu L, Tao Y, Yang H (2011) Synthesis and properties of magnetic and luminescent Fe3O 4/SiO2/YVO4:Eu3+ nanocomposites. Solid State Sci 13:361–365

83. Zhang F, Braun GB, Pallaoro A, Zhang Y, Shi Y, Cui D, Moskovits M, Zhao D, Stucky GD (2012) Mesoporous multifunctional upconversion luminescent and magnetic "Nanorattle" materials for targeted chemotherapy. Nano Lett 12:61–67
84. Yang P, Quan Z, Hou Z, Li C, Kang X, Cheng Z, Lin J (2009) A magnetic, luminescent and mesoporous core-shell structured composite material as drug carrier. Biomaterials 30:4786–4795
85. Peng H, Liu G, Dong X, Wang J, Xu J, Yu W (2011) Preparation and characteristics of Fe3O4@YVO 4:Eu3+ bifunctional magnetic-luminescent nanocomposites. J Alloys Compd 509:6930–6934
86. Peng H, Cui B, Li L, Wang Y (2012) A simple approach for the synthesis of bifunctional Fe 3O 4@Gd 2O 3: Eu 3+ core-shell nanocomposites. J Alloys Compd 531:30–33
87. Beltran-Huarac J, Guinel MJF, Weiner BR, Morell G (2013) Bifunctional Fe3O4/ZnS: Mn composite nanoparticles. Mater Lett 98:108–111
88. Yu W, Ma Q, Li X, Dong X, Wang J, Liu G (2014) One-pot coaxial electrospinning fabrication and properties of magnetic-luminescent bifunctional flexible hollow nanofibers. Mater Lett 120:126–129
89. Ma Q, Wang J, Dong X, Yu W, Liu G (2014) Electrospinning fabrication and characterization of magnetic-upconversion fluorescent bifunctional core-shell nanofibers. J Nanoparticle Res 16:2239
90. Xue H, Sun X, Bi J, Wang T, Han J, Ma Q, Han L, Dong X (2015) Facile electrospinning construction and characteristics of coaxial nanobelts with simultaneously tunable magnetism and color-tuned photoluminescence bifunctionality. J Mater Sci Mater Electron 26:8774–8783
91. Zhou X, Ma Q, Yu W, Wang T, Dong X, Wang J, Liu G (2015) Magnetism and white-light-emission bifunctionality simultaneously assembled into flexible Janus nanofiber via electrospinning. J Mater Sci 50:7884–7895